Supplementary Information:

Table S1 | Summary of primer sequences used in molecular cloning.

Name	Sequence
ACP-forward	5′-GCGCGCGCCATATGAGCACTATCGAAGAACGC-3′
ACP-reverse	5′-TTTAAATTCTCCTTCCCGGGCCCGGTCACGCCTGGTGGCCGTT-3′
ACPS-forward	5′-CCGGGCCCGGGAAGGAGAATTTAAAATGGCAATCTTAGGTTTAGGC-3′
ACPS-reverse	5′-GCGCGCGCCTCGAGTCAACTTTCAATAATTACCGT-3′

The underlined letters indicate the restriction sites for *NdeI* and *XhoI* endonucleases. The bold letters indicate the sequence of the template gene. The green and blue letters show the sequence of the translation spacer element and ribosome binding site, respectively. Orange letters represent the spacer sequence.

Table S2 | Data collection and refinement statistics.

	Intact-Acyl-ACP (His239Ala-LpxD)	*Hydrolyzed-Acyl*-ACP (wild-type-LpxD)	*Holo*-ACP (wild-type-LpxD)
Data collection*			
Space group	*P*1	*P*1	*P*1
Cell dimensions			
a, *b*, *c* (Å)	84.30, 89.44, 112.25	84.18, 89.31, 111.93	89.47, 93.23, 114.30
α, β, γ (°)	104.06, 92.40, 118.47	104.09, 92.58, 118.64	75.93, 73.81, 58.95
No. of Reflections	561496	235456	858856
No. of Unique Reflections	154031	59734	160164
Resolution (Å)	50-2.10 (2.14-2.10)	50-2.90 (2.95-2.90)	50-2.15 (2.19-2.15)
R_{sym} or R_{merge}	0.10 (0.40)	0.09 (0.19)	0.09 (0.64)
I / σI	14.6 (2.3)	13.8 (5.6)	21.9 (1.9)
Completeness (%)	97.7 (94.9)	98.3% (91.1)	96.1 (85.6)
Redundancy	3.6 (3.1)	3.9 (3.7)	5.4 (4.0)
Refinement			
Resolution (Å)	43.38–2.10	28.43–2.89	35.89–2.13
No. reflections	145543	57571	159778
R_{work}/ R_{free} (%)	16.8 / 21.6	20.4 / 25.3	17.8 / 21.6
No. atoms / *B*-factors			
LpxD	14835/39.1	14688/39.3	14914/32.1
ACP	3433/79.9	2631/78.6	2438/79.5
β-OH-C_{14}-4′-PPT	222/43.0	—	—
β-OH-C_{14}OOH	—	136/36.5	—
4′-PPT	—	126/37.3	126/54.6
Water	920/42.5	145/30.4	885/34.8
R.m.s deviations			
Bond lengths (Å)	0.01	0.01	0.01
Bond angles (°)	1.05	0.97	1.03
Ramachandran statistics			
Favored (%)	97.6	97.1	98.1
Disallowed (%)	0.0	0.0	0.0

Data were collected from a single crystal for each complex.
*Highest resolution shell is shown in parenthesis.

Supplemental Figures

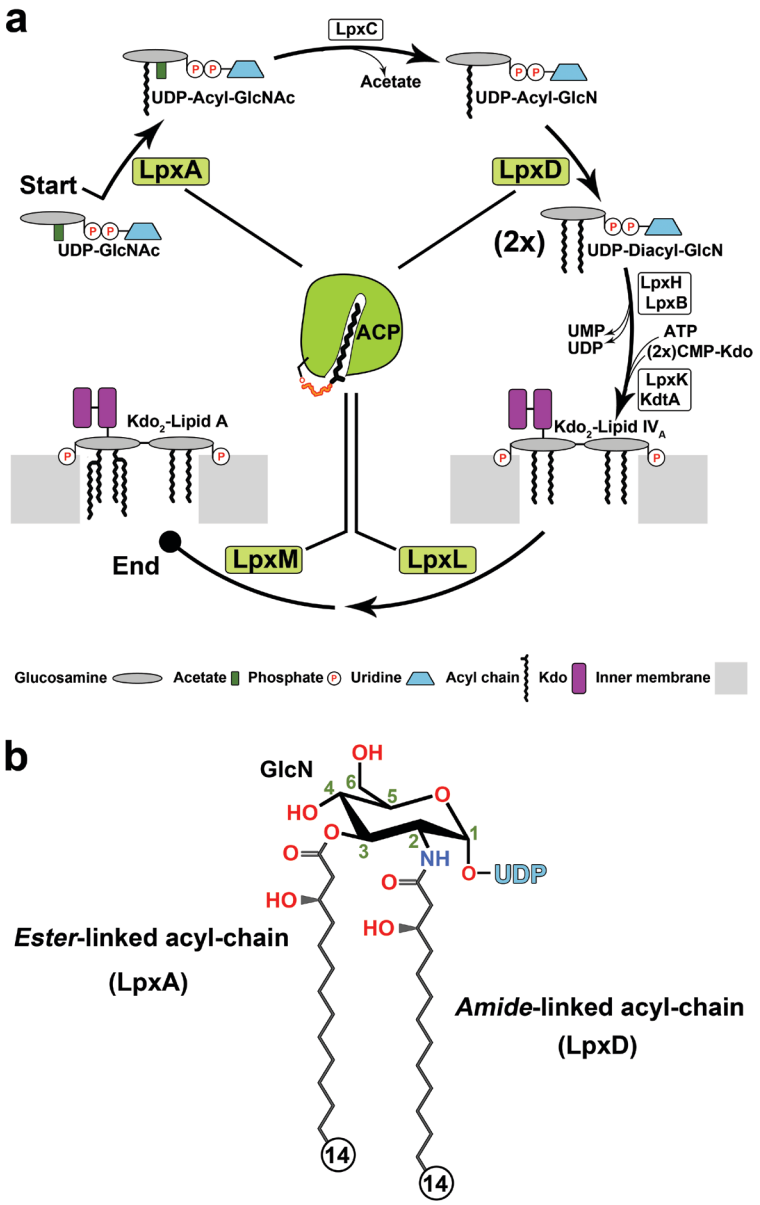

Figure S1 | Biosynthesis of Kdo_2-lipid A in *E. coli*. (**a**) Nine constitutive enzymes (Lpx) and *acyl*-ACP (green) coordinate to assemble Kdo_2-lipid A (Kdo, 3-deoxy-D-*manno*-oct-2-ulosonic acid). Two equivalents of UDP-diacyl-GlcN, as indicated by (2x), are required to generate Kdo_2-Lipid IV_A, which represents the tetra-acylated disaccharide decorated with two Kdo sugars. Highlighted are the four ACP-dependent acyltransferases (green boxes). (**b**) Chemical structure of the LpxD reaction product, UDP-diacyl-GlcN. Acyl-transfer occurs at the 2-position of the GlcN ring, generating an *N*-linked *β-OH-*C_{14} substituent.

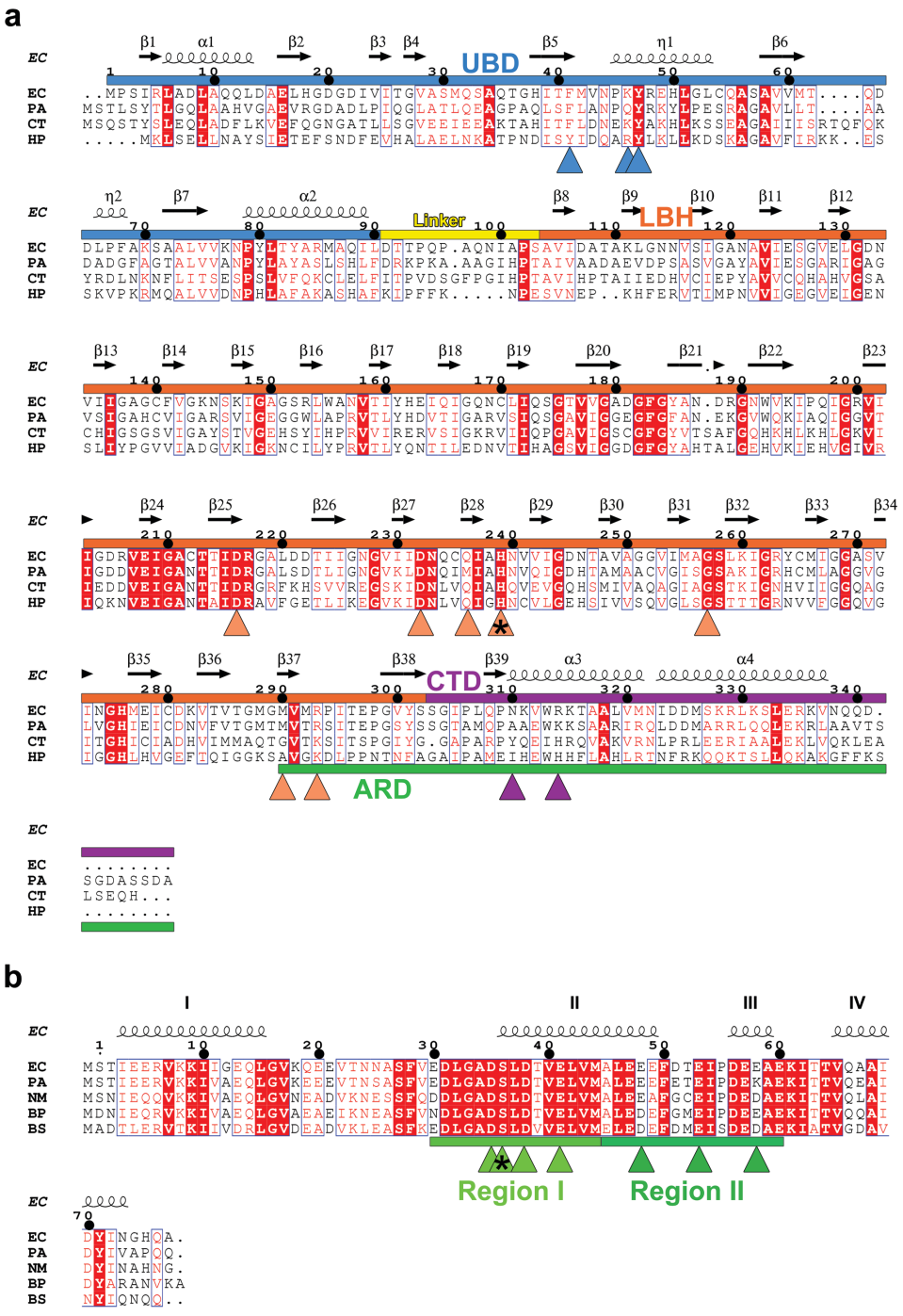

Figure S2 | Sequence alignment of LpxD and ACP homologs. Secondary structure assignment and residue numbers are presented above and are for *E. coli* LpxD or ACP. Red boxes indicate strictly conserved residues and red single letter amino acids show those that are partially conserved. (**a**) The amino acid sequence alignment of *E. coli* (EC) LpxD with *Pseudomonas aeruginosa* (PA), *Chlamydia trachomatis* (CT), and *Helicobacter pylori* (HP). The Blue, yellow, orange, and purple bars above the aligned sequences indicate the uridine binding domain (UBD),

linker region, left-handed β-helix domain (LβH), and the C-terminal domain (CTD), respectively. The ACP recognition domain (ARD) is indicated by a green bar and is presented below the alignment. Residues that contribute to catalysis and substrate specificity are indicated by triangles that are color matched according to domain association; the catalytic His293 is indicated with an asterisk. The Met290 residue which serves as the molecular 'hydrocarbon ruler' for *E. coli* LpxD is also indicated. Although this is indeed the case for *E. coli* LpxD, orthologs often have other chain-length specificity and, thus require fine-tuning of the 'hydrocarbon ruler,' for example with *C. trachomatis* LpxD which incorporates a twenty-carbon acyl-chain[12]. (**b**) Amino acid sequence alignment of ACPs from *E. coli* (EC), *Pseudomonas aeruginosa* (PA), *Neisseria meningitidis* (NM), *Burkholderia pseudomallei* (BP), and *Bacillus subtilis* (BS). The primary sequence of ACP begins with methionine, which for historical reasons (i.e. due to aminopeptidase action) is numbered zero and the serine that is next in sequence is denoted number one. Regions I and II are indicated by light and dark green bars, respectively. Key residues that make strong electrostatic interactions within regions I and II are indicated by triangles that are color matched according to their acidic region association. An asterisk indicates the canonical phosphopantetheinylated serine (Ser36) residue.

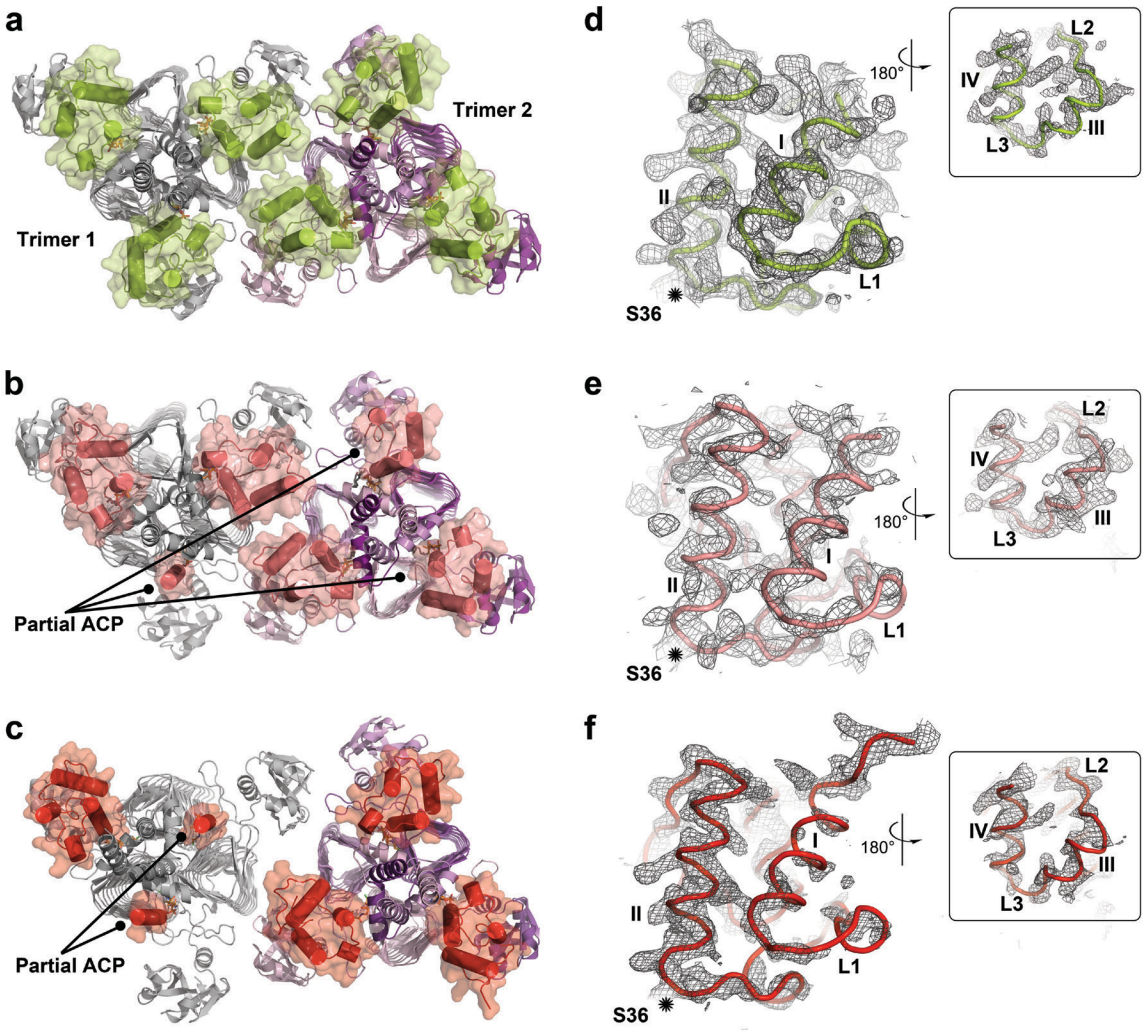

Figure S3 | The asymmetric unit contents of the (**a**) *intact-acyl*-ACP (**b**) *hydrolyzed-acyl*-ACP and (**c**) *holo*-ACP structures in complex with LpxD. Two trimers of LpxD (gray or colored as in figure 1) were observed in the triclinic unit cell. Six molecules of ACP were completely modeled in the *intact-acyl*-ACP structure (green with transparent molecular surface). In the *hydrolyzed-* and *holo*-ACP structures (salmon or red with transparent molecular surfaces, respectively) four molecules of ACP were fully modeled and the remaining two were partially built. Representative molecules of (**d**) *intact-acyl*-ACP (chain H) (**e**) *hydrolyzed-acyl*-ACP (chain J) and (**f**) *holo*-ACP (chain J) with $2F_o - F_c$ composite omit electron density covering each α-carbon trace, contoured at 0.9 σ. (inset) Rotated view showing the backside of ACP.

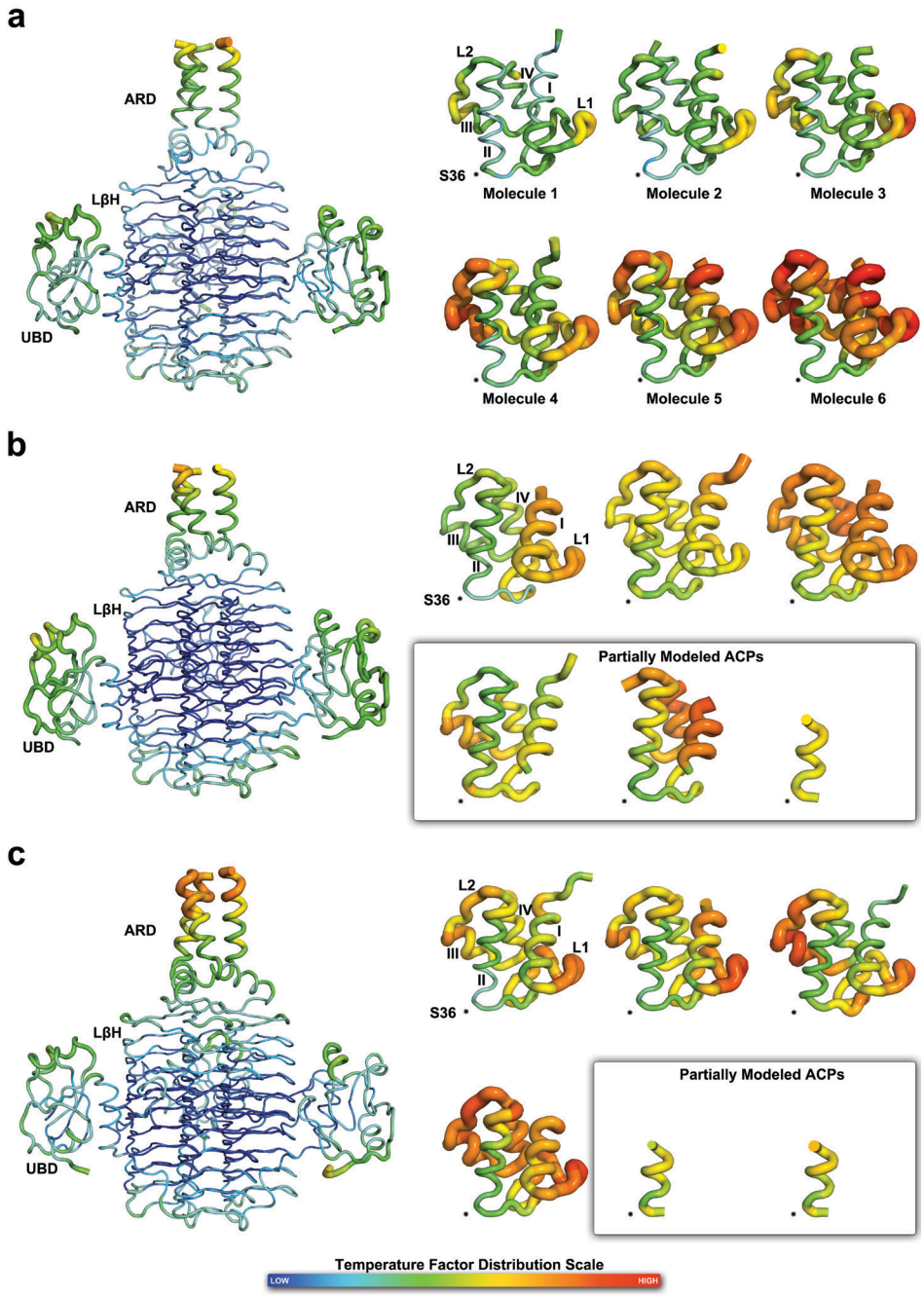

Figure S4 | Temperature factor distribution of LpxD and ACP between the (**a**) *intact-acyl*-ACP, (**b**) *hydrolyzed-acyl*-ACP, and (**c**) *holo*-ACP co-crystal structures. A single trimer of LpxD and all bound ACPs observed in the triclinic unit cell are represented as ribbon-putty diagrams and colored according to main-chain B-value. A scale bar is indicated for the thermal distribution. The subdomains of LpxD are indicated. The location of the pantetheinylated Ser36 residue is indicated with an asterisk symbol and the first ACP molecule of each co-crystal structure is labeled with secondary structural elements. Partially modeled *hydrolyzed*- and *holo*-ACPs are accented with a box.

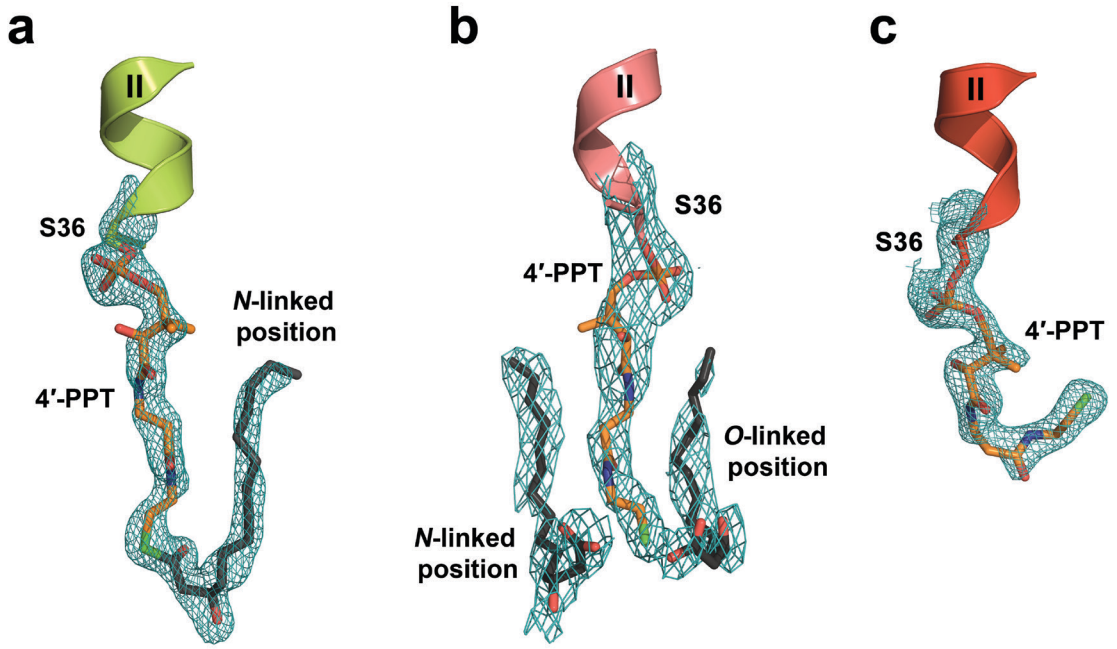

Figure S5 | 4′-PPT and *β-OH-C*$_{14}$ moieties of (**a**) *intact-acyl*-ACP, (**b**) *hydrolyzed-acyl*-ACP, and (**c**) *holo*-ACP that bound in the active site cleft of LpxD. Shown covering Ser36 and the *intact-acyl*-4′-PPT and *holo*-4′-PPT groups is $F_o - F_c$ simulated annealing omit electron density contoured at 3.5 σ. Covering the *hydrolyzed-acyl*-4′-PPT group and the *β-OH-C*$_{14}$ fatty acids is $2F_o - F_c$ composite omit electron density contoured at 1.0 σ.

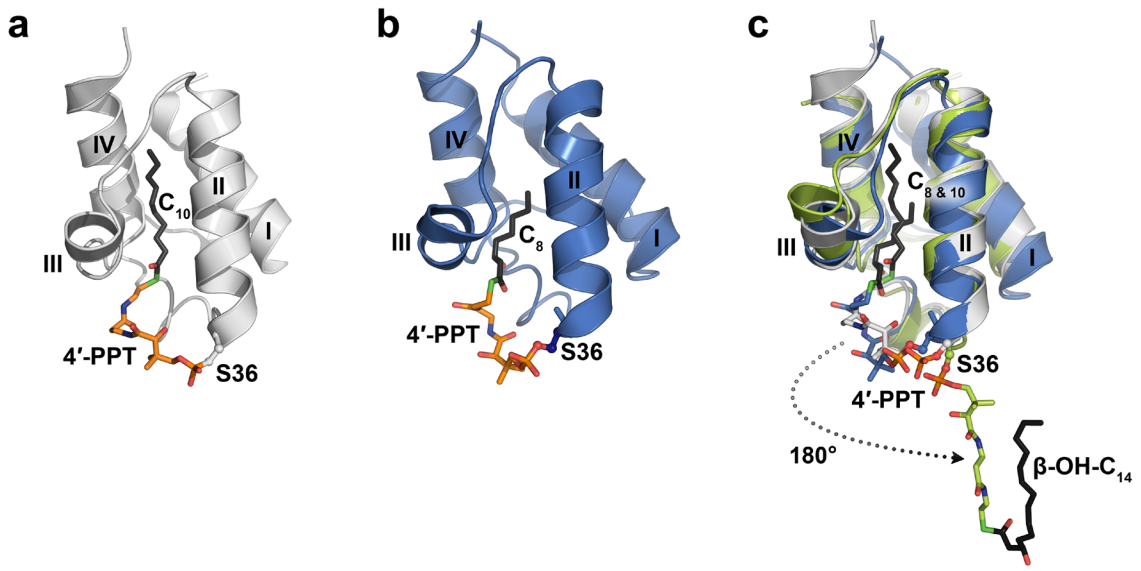

Figure S6 | Structural comparison of *acyl*-ACPs. The X-ray and NMR structures of (**a**) *E. coli* decanoyl-ACP (PDB 2FAE, light gray) and (**b**) *S. coelicolor R*-3-hydroxyoctanoyl-ACP (PDB 2KOQ, blue), respectively, determined in the absence of partner enzyme. The acyl-chains (dark gray) are covalently attached via a thioester bond to the 4′-PPT arm (colored in orange and by atom) and are tucked inside the hydrophobic cavity. (**c**) Superposition of decanoyl- and *R*-3-hydroxyoctanoyl-ACP with the structure of *intact-acyl*-ACP colored green (LpxD is omitted for simplicity). The 4′-PPTs are colored according to ACP affiliation. The 4′-PPT arm of *intact-acyl*-ACP has pivoted about Ser36, rotating by 180° rotation to present the acyl-chain to the active site of LpxD.

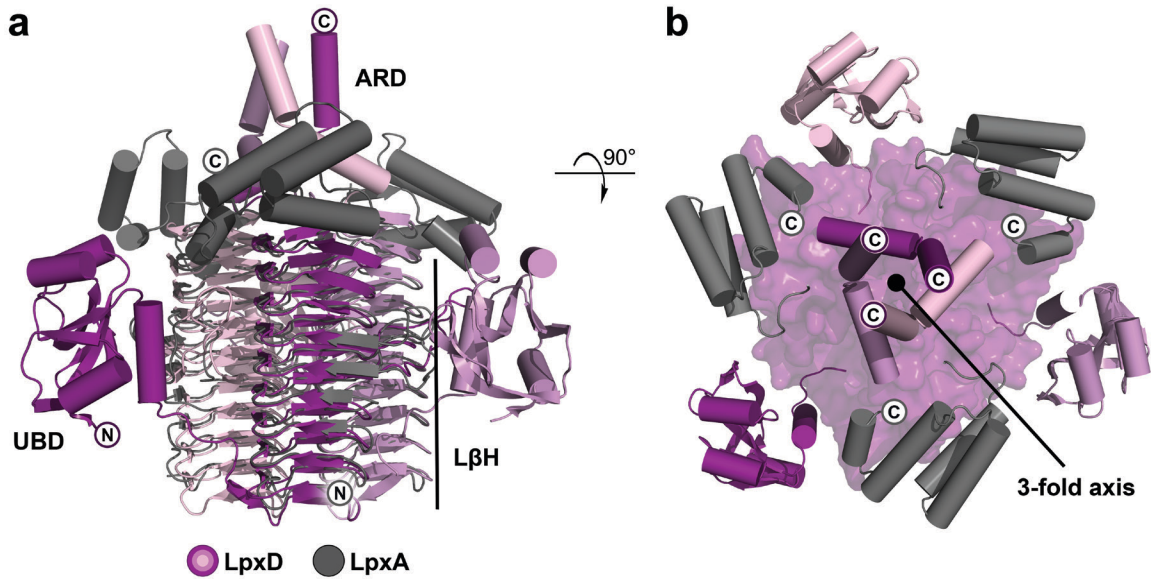

Figure S7 | Structural comparison between the functionally related LpxD and LpxA acyltransferases. (**a**) Similar to LpxD (purple), LpxA (PDB 1LXA, gray) is a homotrimer. The UBD module of LpxD has no equivalent counterpart in the LpxA structure. The LβH domains superimpose well and show an equal number of β-helical-coils between them. (**b**) Rotated view by 90° from that shown in panel A highlighting the differences between the C-terminal regions. Molecular surface is shown covering the LβH domains of LpxD. The ARD of LpxD interdigitates and forms a 3-helix bundle. Analogous helices of LpxA are collapsed and instead interact with their respective monomer.

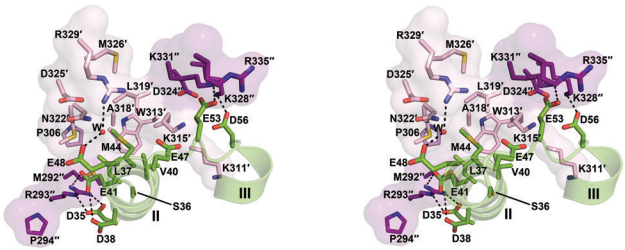

Figure S8 | Stereoview of the *intact-acyl*-ACP complex. Only those residues and their molecular surfaces that contribute at the protein-protein interface (chain I) are shown. Salt-bridge interactions are indicated by black dashes. The *acyl*-4′-PPT group attached to Ser36 is omitted for clarity.

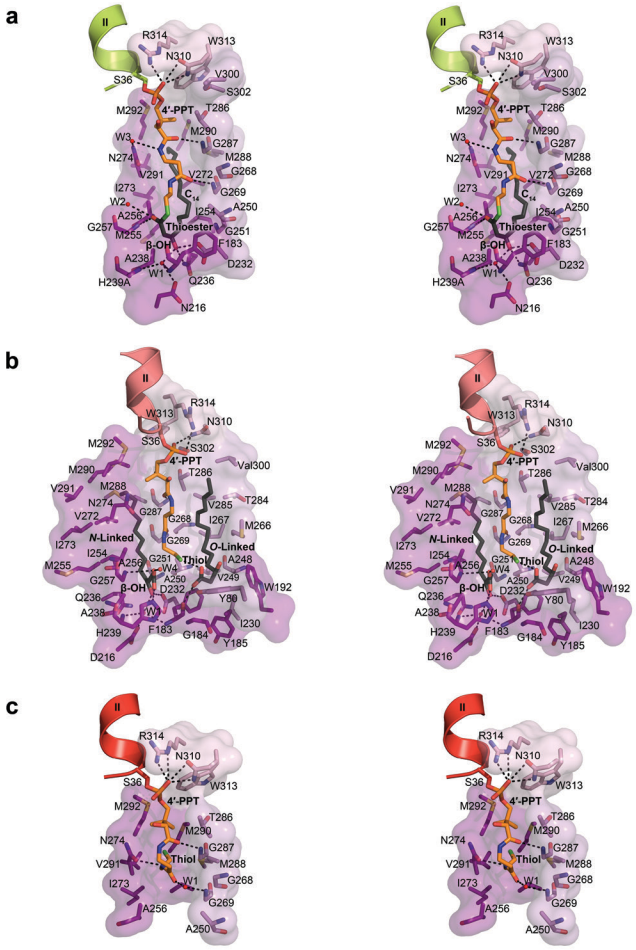

Figure S9 | Stereoview of (**a**) *intact-acyl*-ACP, (**b**) *hydrolyzed-acyl*-ACP, and (**c**) *holo*-ACP complex structures detailing the interaction of the acyl-4′-PPT moieties within the reaction chamber of LpxD. Only those residues that contribute to ligand contact are shown with transparent molecular surfaces. Hydrogen bonds are shown as black dashes and the color scheme is as in figure 1 and 2.

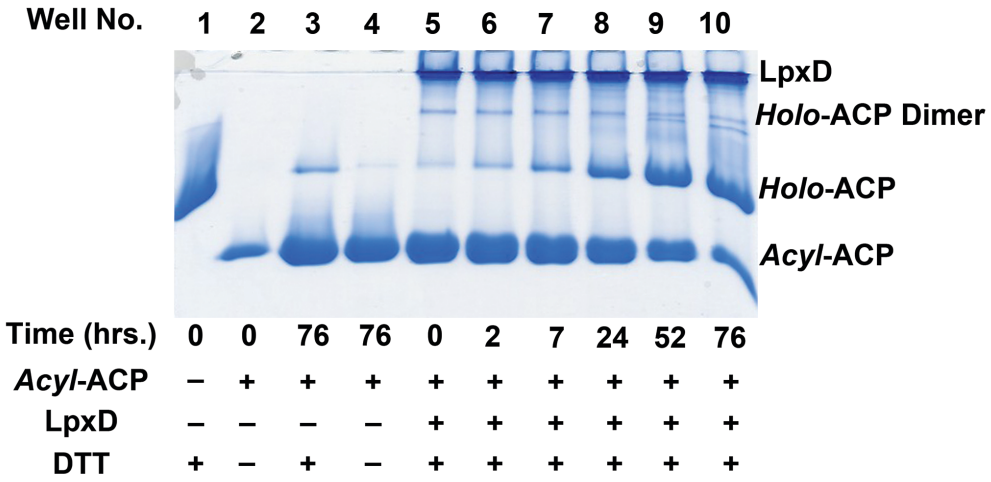

Figure S10 | Evidence for the hydrolysis of *acyl*-ACP. Conformationally sensitive 2.5 M urea polyacrylamide (19%) gel-shift assay investigating the cleavage of the thioester bond of *acyl*-ACP in the presence (+) or absence (–) of 0.3 mM DTT and LpxD as a function of time. The assay mixture and temperature were kept consistent with the solution used for crystallization (0.1 M MES pH 6.5, 0.2 M ammonium sulfate, 20% PEG 8000, and incubation at 15 ˚C). The well numbers are indicated above the gel. Lanes 1 and 2 indicate *holo*- and *acyl*-ACP, respectively, and serve as controls. *Holo*-ACP even in the presence of DTT shows a weak, higher molecular weight band that corresponds to a disulfide bound form of holo-ACP via the pantetheinyl arm. Lanes 3 and 4 indicate the effect of DTT alone on *acyl*-ACP after 76 hours. Lanes 5 through 10 show *acyl*-ACP in the presence of both DTT and LpxD at the indicated time points. The data indicate an enhancement of *acyl*-ACP hydrolysis by DTT and LpxD.

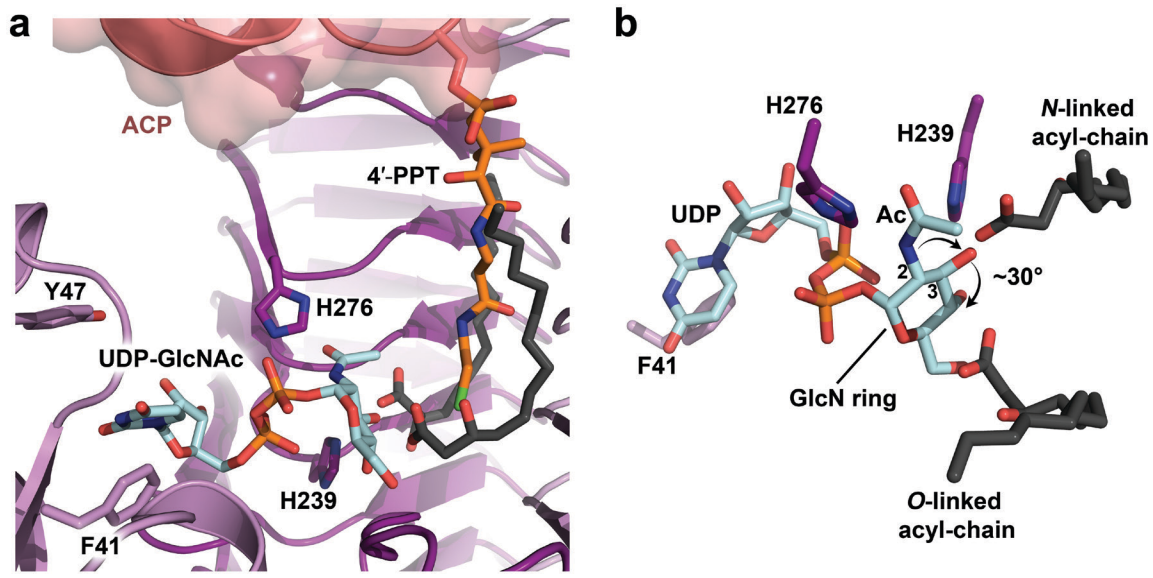

Figure S11 | Comparison between the *E. coli hydrolyzed-acyl*-ACP complex and LpxD from *C. trachomatis* bound to UDP-GlcNAc (PDB 2UIA). (**a**) Close-up view of the binding of UDP-GlcNAc (cyan, colored by atom) in the catalytic cleft of LpxD. The position of the UDP-GlcNAc relative to the nucleotide binding pocket, His239, the acyl-chains within the *N*- and *O*-channels, and the *hydrolyzed*-4′-PPT arm is shown. For clarity, the cartoon representation of *Ct*LpxD is not shown. (**b**) Rotated view showing the orientation of the GlcNAc ring. A ~30° clockwise rotation (arrow) is needed for the attachment sites of both acyl-chains to properly align with their respective carboxylate head groups, i.e. the 2- and 3-positions of GlcNAc.

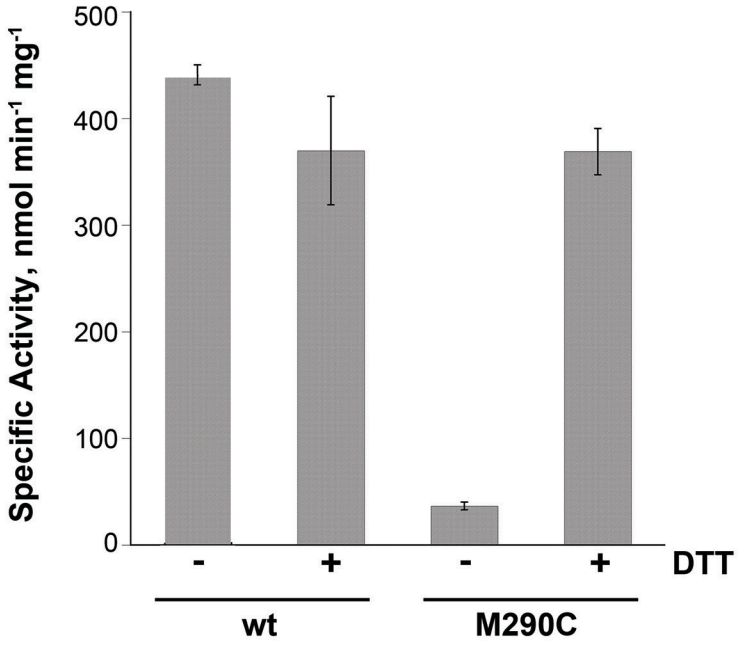

Figure S12 | Biochemical evidence for the role of ACP in product release. Bar chart showing the effects of DTT on the *in vitro* specific activity of wild-type LpxD (wt) or the Met290Cys (M290C) LpxD mutant. The assay mixture contained 40 mM HEPES (pH 7.4), 0.02 mg/mL BSA, 6 μM *β-OH-*C_{14}-ACP, and 4 μM [α-^{32}P]-UDP-acyl-GlcN (0.005-0.04 μCi/μL). The reaction was initiated by the addition of either 1.4 nM wild-type *E. coli* LpxD or 4.2 nM Met290Cys LpxD enzyme. Compared to wild-type enzyme, the cysteine mutation abrogates activity, although the data do indicate a small, but measurable turnover. The addition of reductant to the assay mixture (rescues the Met290Cys mutant, within error, to near wild-type levels of activity assayed in the presence or absence of DTT. Each column (gray bars) are plotted as the mean value of the data, *M*, with an $n = 3$ in each case. Range error bars are displayed that describe the amount of spread between the extremes of the data and were calculated by subtracting the lowest point from the highest.

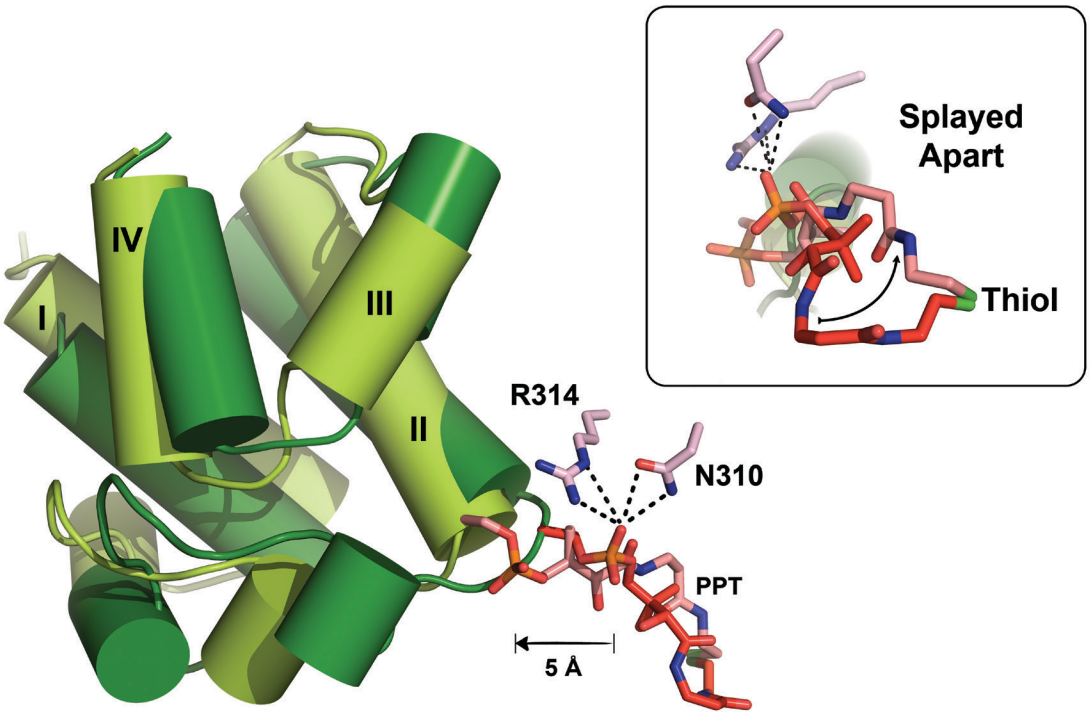

Figure S13 | Structural differences between molecules of *holo*-ACP. The superimposed *holo*-ACPs are colored light (chain I) or dark green (chain K) and their 4′-PPT groups are colored salmon or red, respectively. All four helices have displaced from one another. The 4′-PPT group (chain I) shifts by ~5 Å and splays apart from chain K (inset, rotated 90°). The terminal thiols remain affixed at the far end of the *N*-channel near Met290, identical to the other molecules of *holo*-ACP.